MAGNETOCALORIC RESPONSE OF NON-STOICHIOMETRIC Ni_2MnGa ALLOYS AND THE INFLUENCE OF CRYSTALLOGRAPHIC TEXTURE

M.V. McLeod[1], A. K. Giri[2,#], B. A. Paterson[3], C. L. Dennis[3], L. Zhou[4], S.C. Vogel[5], O. Gourdon[5], H. M. Reiche[5], K.C. Cho[6], Y. H. Sohn[4], R. D. Shull[3], and B.S. Majumdar[1§]

[1]New Mexico Institute of Mining and Technology, Socorro, NM 87801,USA [2]TKC Global, Herndon, VA 20171, USA, [3]National Institute of Standards and Technology, Gaithersburg, MD 20899,USA. [4]University of Central Florida, Orlando, FL 32816, USA [5]Los Alamos National Laboratory, Lujan Neutron Science Center, Los Alamos, NM 87545, USA. [6]US Army Research Laboratory, MD 21005, USA

[#] Contractor to the US Army Research Laboratory, Aberdeen Proving Grounds, MD 21005, USA

§ Corresponding author

Keywords: magnetocaloric, NiMnGa alloy, polycrystalline, preferred orientation, twinning

Abstract: Currently, there is significant interest in magnetocaloric materials for solid state refrigeration. In this work, polycrystalline Heusler alloys belonging to the $Ni_{2+x}Mn_{1-x}Ga$ family, with x between 0.08 and 0.24, were evaluated for the purpose of finding composition(s) with an enhanced magnetocaloric effect (MCE) close to room temperature. Differential scanning calorimetry (DSC) was successfully used to screen alloy composition for simultaneous magnetic and structural phase transformations; this coupling needed for a giant MCE. The alloy with x = 0.16 showed an excellent match of transformation temperatures and exhibited the highest magnetic entropy change, ΔS_M, in the as-annealed state. Furthermore, the MCE increased by up to 84 % with a 2 Tesla (T) field change when the samples were thermally cycled through the martensite to austenite transformation temperature while held under a constant mechanical load. The highest ΔS_M measured for our x = 0.16 alloy for a 2 T magnetic field change was -18 J/kg-K. Texture measurements suggest that preferential orientation of martensite variants contributed to the enhanced MCE in the stress-assisted thermally cycled state.

1. Introduction

Energy and environmental demands, combined with the observation [1] of a giant magnetocaloric effect (MCE) in a $Gd_5(Si_2Ge_2)$ alloy, have led to a strong interest in MCE materials [1-3]. In particular, these MCE materials are a candidate system for solid state magnetic refrigeration near room temperature (RT).

To date, an observed feature of giant MCE materials is that they exhibit a closely coupled first order structural phase transformation and magnetic ordering/transformation. This coupling may permit a magnetic field to induce a first order structural phase transformation, also known as a magnetostructural transformation [1]. The nature of this field induced transformation has been investigated for Gd_5Ge_4 using in situ X-ray diffraction under magnetic fields [4]. The change in magnetization due to the structural transformation, likely arising from slightly altered bond lengths between atoms with strong magnetic moments, can thus contribute to the measured magnetic entropy change, ΔS_M, and manifest as giant MCE behavior. Indeed, it has been suggested that the measured entropy change is composed of a normal magnetization change for the initial phase, which would be higher at the magnetic phase transition, plus a contribution from the field induced structural transformation [4, 5]. The promotion of the phase with greater magnetization naturally shifts the transformation temperature under a magnetic field, and may be treated using Clausius-Clapeyron relationship. Giant MCE behavior has also been observed in a number of Heusler X_2YZ alloys, where X and Y are 3d transition metal elements; one of which dominates the magnetic moment contribution, and Z is an element in the IIIA to VA group.

In this investigation, we have focused on a class of non-stoichiometric Ni-rich $Ni_{2+x}Mn_{1-x}Ga$ Heusler alloys that have been found to exhibit a giant MCE, while eliminating toxic or rare earth elements. It is interesting to note here that extended solid solubility in the intermetallic phase is a

fairly common feature of giant MCE materials [4, 6, 7]. At specific compositions, the stability of the phases may be compromised enough to permit field induced structural transformation [8]. The non-stoichiometric Ni_2MnGa alloys also demonstrate magnetic shape memory alloy (MSMA) characteristics that resemble thermoelastic shape memory behavior of near stoichiometric NiTi alloys. The elevated temperature austenite phase has the ordered cubic Heusler ($L2_1$) structure, which undergoes a diffusionless martensitic transformation to either an ordered tetragonal ($L1_0$) or an ordered modulated monoclinic (almost orthorhombic) martensitic structure with a lesser degree of symmetry than the parent ordered cubic phase. The atomic magnetic moments are mostly concentrated in the Mn atoms, and an early paper on the subject [9] suggests moments of $4.1\mu_B$ for Mn and $0.3\mu_B$ for Ni atoms, with Ga making a negligible contribution. The preferred orientation of these atomic magnetic moments naturally makes the material highly anisotropic magnetically with respect to crystallographic direction. Together with the mobility of thermoelastic martensite variants (whereby one variant can be replaced by another through a largely dislocation free twinning mechanism), this leads to macroscopic strain and shape changes upon application of a magnetic field [10-12]. In the context of the MCE, suitable alignment of the martensite variants to enhance magnetization could be utilized to increase the MCE.

In NiTi, the rearrangement of martensite variants is such that the material performs maximum work [13, 14], with maximum strain tending to occur in the direction of load to minimize the potential energy of the system. Texture measurements and strains associated with Bain transformations confirm that the microstructure responds in this manner on application of a load [15-18]. Moreover, if the material is held slightly above the austenite finish temperature, then application of a load can induce the structural transformation from the austenite to the

martensite phase, i.e., a stress-induced structural transformation. Thermodynamically, a magnetic field induced structural transformation is similar to this behavior [2].

The influence of a magnetic field on structural phase transformations depends sensitively on the composition. Here, the Ga level was kept constant. The objectives of this research were the following: (1) optimize compositions that provide simultaneous crystallographic and magnetic transformations close to RT for refrigeration applications, and (2) enhance the magnetocaloric performance through prior processing. Since only one parameter in the composition space (x) is varied, the study permits improved understanding of structural phases and magnetic order at the atomic scale.

For convenience, the MCE was assessed based on the isothermal magnetic entropy change, ΔS_M, while recognizing that this parameter may not be as good an indicator of magnetic refrigeration potential as the isentropic temperature change, ΔT_{ad} [7, 19]. The principal Maxwell equation relating the magnetic entropy change to the magnetization is as follows:

$$\left(\frac{\partial S}{\partial H}\right)_T = \left(\frac{\partial M}{\partial T}\right)_H$$

From this it follows that $\Delta S_M = \int_0^H \left(\frac{\partial M(H,T))}{\partial T}\right)_H dH$. This relation can be calculated by measuring M versus T for several constant values of H, doing the derivative $\left(\frac{dM}{dT}\right)_H$ as a function of T, and then integrating those values over H. Alternatively, this relationship could be determined by pulling the derivative outside the integral to obtain the following –

$$\Delta S_M = \frac{\partial}{\partial T}\left[\int_0^H M(H,T)dH\right]$$

Then, from measurements of M versus H at constant temperature, measured at several temperatures, the integral MdH can be evaluated and then differentiated with respect to T to

obtain ΔS_M. Because of the much longer times required to change and stabilize temperature than to change and stabilize the field in a magnetometer, we like most of the magnetic community have chosen to evaluate ΔS_M by this so-called "standard" method [20]. For systems possessing magnetic and thermal hysteresis, as in the system of this work, neither of these techniques, nor variations on them [20], is exact, and the value of ΔS_M (referred to as the MCE of the material) must be considered as only approximate. Even still, they may be used for making comparisons between similar materials.

In previous work on the MCE in polycrystalline samples of Ni-rich non-stoichiometric Ni_2MnGa alloys, ΔS_M values ranged from -5 to -20 J/kg-K for a field change of 1.6 T [21]. In other related work, a magnetic entropy change of -96 J/kg-K were reported for a polycrystalline $Ni_{2.2}Mn_{0.74}$ Ga alloy for a 5 T field change, although significant hysteresis was observed in the magnetization curves [22]. In a separate work on a single crystal (SX) of a Ni-rich Ni_2MnGa alloy, the isothermal ΔS_M value was found to be as high as -86 J/kg-K for a field change of 7 T, although Clausius-Clapeyron relations yielded a much lower value of -24 J/kg-K [23]. The difference was ascribed to the large variations in the specific heat (C_p) during the first order transformation and the influence of magnetic field on C_p. Later research by the same group found that the isothermal entropy was reduced almost by a factor of 10 for a polycrystalline sample, although the polycrystalline and SX samples had compositional differences [24]. The SX sample also exhibited superelastic behavior whereby the austenite became unstable under stress and converted to martensite at a temperature slightly above the martensite start temperature. Unfortunately, fabrication difficulties and scale-up considerations limit the use of SX material in large scale applications; therefore, in this work, an attempt has been made to impart preferential texture in polycrystalline specimens for an improved MCE.

In [17, 18], thermal cycling of NiTi polycrystalline samples at constant stress was shown to impart strong texture in the martensite at a stress level well below that for texture changes associated with deformation in the martensite state, i.e., at stresses below the martensite detwinning plateau stress. The low elastic shear modulus along the [110] direction, characterized by C' (where C' = $[C_{11}-C_{12}]/2$ and C_{11} and C_{12} have the standard nomenclature for elastic stiffness constants along <100> directions) at the phase transformation temperature, contribute to the low stress required to bring about preferred orientation of the martensite variants [18, 25]. Guided by these results and the thermoelastic character of Ni_2MnGa alloys, a similar approach was adopted here, since a low stress could be utilized without cracking the brittle intermetallic alloy. Indeed, sharp reductions in shear modulus C' have also been observed in Ni_2MnGa alloys at the phase transformation temperature and are believed to be due to magnetoelastic interactions [26, 27]. Preliminary results from this research were reported in [28] wherein significant enhancements in the MCE following thermal cycling under load were observed. In this paper, additional results are presented especially on texture measurements, which provide insight on the role of preferred orientation of martensite variants on the MCE enhancement.

2. Experiments

2.1 *Specimen Preparation*:

Polycrystalline $Ni_{2+x}Mn_{1-x}Ga$ alloy buttons of approximate weight 15 g were triple arc melted in argon with starting compositions ranging from x = 0.08 to x = 0.24. The compositions were selected to cover a broad range of electron to atom (e/a) ratios, in an effort to select compositions with close proximity of the structural and magnetic transformation temperatures. These compositions are listed in Table 1, along with actual compositions determined by Luvak Inc. [DISCLAIMER] using direct current plasma emission spectroscopy (DCPES) for some of

the alloy samples. The typical weight loss was about 0.5 percent during arc melting. Homogenization of the crown-top billets/buttons (approximately 35 mm in diameter and 10 mm in height at the center) was conducted in 1.3×10^{-4} Pa (10^{-6} Torr) vacuum at 1273 K for 72 hours and furnace cooled. At 1273 K, the alloy has a B2 crystallographic texture which promotes rapid diffusion and homogenization. The buttons exhibited a highly columnar structure directed from the bottom copper chill to the top surface of the billet. Multiple approximately 4 mm cube samples for structural and magnetic characterization and thermal cycling were sliced using a low speed diamond saw from the central height section of the billet, and the faces were mechanically polished to remove imperfections from the saw cutting procedure. The magnetic measurements required an additional sectioning process (also using a low speed diamond saw) to produce a sample approx. 1 mm x 2 mm x 4mm with the columnar growth direction parallel to the 4mm side. Subsequent mechanical load or magnetic field was directed along the columnar growth direction.

2.2 *Specimen Characterization*

The phase transformation temperatures and enthalpy of structural transformation were measured using a Perkin Elmer DSC apparatus [DISCLAIMER]. A ramp rate of 10 K/min was used for the DSC scan. Heat capacity (C_p) measurements were also performed using modulated DSC on a TA Instruments Q2000 model [DISCLAIMER], and detailed results will be presented in a separate publication. Crystal structures and lattice parameters were determined using neutron diffraction. Preferred crystal orientation effects and the presence of only a few peaks posed problems in accurate characterization of the martensite crystal structures from X-ray measurements. Therefore, neutron diffraction experiments were conducted on the powder diffractometer POWGEN at the SNS site of the Oak Ridge National Laboratory. Cube samples

as well as crushed and annealed powders from the arc melted buttons were encased in vanadium cans and then probed by neutron diffraction measurements. Rietveld refinement using the GSAS software [29] [DISCLAIMER] was utilized to determine the lattice parameters, and in some instances preferred orientation was invoked to account for texture in the as-fabricated state.

A more accurate estimate of texture was obtained using the neutron time of flight (TOF) diffractometer HIPPO (high pressure preferred orientation) goniometer at the Los Alamos Neutron Science Center (LANSCE) [30, 31]. HIPPO utilizes approximately 1200 ^{3}He detector tubes arranged on 50 detector panels positioned on rings at five different diffraction angles around the incident beam direction so that each detector probes a different sample direction. For each texture measurement the sample is rotated around the vertical axis (perpendicular to the incident neutron beam) into three positions (0°, 67.5°, 90°) to increase pole figure coverage. At each position, data were collected for 15 minutes. The samples were aligned such that the incident beam was along the columnar axis of the grains. The data were analyzed using the MAUD program [32, 33] [DISCLAIMER] following procedures described in [34]. In the pole figures presented here, the beam and columnar growth directions are along the center of the pole figures (perpendicular to the page). The other two directions that are perpendicular to this axis in the pole figures are therefore transverse to the columnar grain axis.

The magnetic measurements were performed using a superconductive quantum interference device (SQUID) magnetometer by Quantum Design [DISCLAIMER]. The magnetization (M) vs. temperature (T) data were the first magnetic measurements performed on the samples after the indicated treatments and were measured with increasing temperature while holding the field constant at a nominal applied magnetic field ($\mu_0 H$) of 0.1 T. The Curie temperature (T_C) was determined from the inflection point in the M vs. T data. The shape and size of samples were

approximately the same in the as-annealed materials and after stress assisted thermal cycling that are described later. Thus, demagnetization factors are not expected to be substantially different in the samples studied, so that any change due to thermal cycling must represent something intrinsic to the material. The M vs. $\mu_0 H$ data were obtained after the M vs. T measurements. They were measured at fixed temperature (starting at the highest temperature) and decreasing magnetic field (from $\mu_0 H$ = 7 T to 0 T), followed by sequentially cooling to the next lower temperature in zero field and repeating the M vs. $\mu_0 H$ measurement. At three temperatures (the highest, lowest, and near T_C), a full M vs. $\mu_0 H$ loop was measured from +7 T to -7 T and back to +7 T to check for hysteresis. For these three temperatures, the temperature change took place under a 7T field instead of zero field, and the hysteresis was negligible. Maxwell's relation was used to determine ΔS_M from the M vs. $\mu_0 H$ data at different temperatures [28]. We note that an alternate "loop" method has been proposed in the past [20] to account for the history dependence of volume fraction of paramagnetic and ferromagnetic states when there is large thermal hysteresis. As indicated earlier, we have preferred to use the so called "standard" method [20], which should provide adequate assessment on the role of preferred orientation of the martensite on the MCE of the different alloys.

In order to enhance the magnetostructural coupling in the polycrystalline material, one of the approximately 4 mm cube samples of each alloy was thermally cycled from below the martensite finish (M_f) to above the austenite finish (A_f) temperatures, under a compressive stress of about 20 MPa along the columnar growth direction. This was also the magnetization axis for subsequent magnetic measurements. The magnitude of stress was dictated by the load capability of the material because higher applied stresses led to cracking of the sample and, as indicated earlier, the low shear modulus at the transformation temperature helps keep the stress level low.

The preferred crystallographic orientation of the samples after cycling would reflect a shortening of the sample in response to a compressive stress through a twinning mode of deformation, similar to other alloys that undergo thermoelastic martensitic transformations [13, 18]. Since the shortest crystallographic axis (either 'c' or 'a' in reference to the tetragonally distorted form of the parent ordered cubic austenite structure) is found to coincide with the easy magnetization axis in single crystal MSMA work on non-modulated/5M/7M martensitic structures [11, 35], a potentially larger magnetization and therefore MCE could be obtained after thermal cycling.

The samples were thermally cycled under load approximately 10 times, with the objective that such 'training' would establish a favorably aligned martensite structure and possibly enhanced twin mobility, as these are difficult to achieve using a magnetic field alone. For example, simple mechanical cycling has been shown to enhance twin mobility in single crystal Ni_2MnGa MSMAs, as evidenced from lower twinning stress [11, 36]. Among possible mechanisms, it has been suggested that predisposed dislocations that nucleate and grow during movement of favorably oriented twins contribute towards preferred orientation of martensite following 'training' in NiTi shape memory alloys [37, 38].

A sketch of the equipment utilized in constant stress thermal cycling is shown in Figure 1. Heating and cooling in this apparatus were accomplished by a cartridge heater and passing a coolant from a chiller, respectively. Thin (0.1 mm thick) and hard stainless steel foils were placed between the sample and the aluminum-alloy platens, and sensitive thermocouples were spot welded to these foils within 2 mm of the sample to permit local temperature measurements. A compressive load was applied at RT and held constant during cycling using an MTS servohydraulic load frame [DISCLAIMER].

Limited transmission electron microscopy (TEM) was conducted using a FEI^{TM} Tecnai F30 [DISCLAIMER] on both the uncycled and stress assisted thermally cycled samples. The TEM analysis provided added information on the crystal structure as well as evidence of intense twinning in the martensite phase.

3. Results

Figure 2 is an optical micrograph of the cross section of a billet and illustrates a columnar grain structure, with grains growing from the flat bottom to the top curved surface of the billet. These prior austenite grains were of the order of 1 mm in length, but were on the average less than 200 μm in the transverse direction. Samples for mechanical and magnetic evaluation were sectioned from the central dominant columnar section of the billet, so as to minimize variability arising from different types of microstructures.

Figure 3a and 3b show the DSC heat flow (endothermic up) data at zero magnetic field for samples x = 0.14 (X2A) and x = 0.16 (X2B), respectively. The DSC data for x = 0.14 shows not only a first order phase transformation at about 315 K, but also a second order transformation that manifests in the form of an inflection point in the heat flow curve at 335 K; actually the curve represents the heat capacity since the temperature ramp rate is constant. The sigmoidal nature of this second order transition can be observed at a higher magnification. The M vs. T data at $\mu_0 H = 0.1$ T is superimposed in Figure 3a. The location of the T_C (defined as the mid-point in the magnetization drop) is estimated at 335 K and confirms that the ferromagnetic to paramagnetic transition coincides with the second order transformation temperature in the DSC plot, consistent with the second order nature of this magnetic transition. It is also important to note that T_C does not change as a function of applied magnetic field, within the range of 0.01-1

T, despite the existence of magnetic field induced structural transitions. Therefore, the M vs. T measurements is assumed to not structurally change the sample. For most of the alloys, this second order phase transition temperature could be resolved and form the basis for estimating the T_C from the DSC plots. The exceptions were samples x = 0.16 and x = 0.19, which did not exhibit a clear cut second order transformation, although the cooling portion of the x = 0.16 sample (Fig. 3b) does appear to indicate a shoulder in the DSC plot just below the M_s temperature. Since this temperature is almost identical to the measured Curie temperature (T_C) of 340 K, we may once again see a good agreement between the T_C and the DSC based second order phase transformation temperature.

The start and finish transformation temperatures and enthalpy of transformation for the samples are listed in Table 2, where DSC data from stress-assisted thermally cycled samples (marked SATC) are also included. The enthalpies and the average entropies of structural transformation during cooling appeared to reach a maximum when x = 0.16, the alloy composition at which the magnetic and structural transformations were coincident. Furthermore, the entropy of structural transformation for this alloy showed an increase following SATC.

The thermal and magnetization data for the alloys are incorporated into a phase diagram shown in Figure 4. The DSC peak temperatures for the first order martensitic transformation on cooling, which approximates the martensite-start temperature (M_s), are plotted as red-squares versus the nominal x-values in the formula $Ni_{2+x}Mn_{1-x}Ga$. The e/a ratios are indicated on the top since they have been commonly used to delineate composition regimes for different martensitic structures [10]. Also plotted with solid diamond symbols in Fig. 4 are DSC based second order phase transformation temperatures. The T_C value was determined from the magnetization data

for x = 0.08, 0.14 and 0.16, and they are plotted in Figure 4 with open circle symbols. It can be seen that the estimated second order phase transformation temperatures from DSC are in good agreement with measured T_C values. Thus, DSC data alone may be used for initial alloy screening for simultaneous structural and magnetic transitions.

At x = 0.16, the T_C from magnetic measurements was 340 K, which lay too close to the first order structural transformation and so may explain the absence of second order phase transformation in the DSC data for this material. A similar absence occurred for x = 0.19, which suggests that the T_C for this material may also lie within the first order transformation. Overall, Figure 4 suggests that while the first order transformation temperatures depend strongly on the Ni to Mn ratio or equivalently the e/a ratio, the estimated or measured T_C values are relatively insensitive to the compositions considered here. Austenite is ferromagnetic for $x<0.16$ and paramagnetic for alloys $x>0.19$. Furthermore, an x between 0.16 and 0.19 appears to be an optimum composition for simultaneous structural and magnetic transformations. This optimum composition would change with different Ni to Ga ratios and the addition of other elements. For the alloys analyzed here, the excess Ni atoms above the stoichiometric Ni_2MnGa composition are located at the Mn sub-lattice [39].

Figures 5a and 5b show the RT neutron diffraction data for samples x = 0.14 and x = 0.16, respectively, where both samples were in the martensite state, see Figure 4 for sample x = 0.14. GSAS-based Rietveld refinement indicated that the 7M modulated monoclinic structure (*I12/m1*) with lattice parameters: $a = 4.281$ Å, $b = 5.532$ Å, $c = 4.191$ Å (all with a standard deviation of ±0.001 Å), $\alpha = \gamma = 90°$, *and* $\beta = 91.9°$ fit most of the peaks for sample x = 0.14. However, there were discrepancies in intensities that are believed to be due to strong preferred crystallographic orientation of the martensite. Crushing a different piece of the same billet into a powder followed

by 723 K annealing did not appear to improve the Rietveld fit any significantly. In the case of sample x = 0.16, the martensite was found to possess a non-modulated (NM) tetragonal structure with $a = b = 3.878$ Å, $c = 6.485$ Å (all with a standard deviation of ±0.001 Å). The diffraction pattern in this case was fit with the primitive body centered tetragonal (bct) *I4/mmm* space group with the excess Ni atoms in $Ni_{2+x}Mn_{1-x}Ga$ occupying the Mn sites [39]. Although Figure 5b does not exhibit good profile fitting using the Rietveld technique, we have uploaded an alternate diffraction file (Supplementary Figure S1) as part of our Supplementary Documents for this same alloy condition, but obtained using the neutron preferred orientation diffractometer (HIPPO) at LANL. The multiple detector banks on this texture measurement apparatus capture different intensity profile for each bank, and Figure S1 shows that for certain banks, and for specific orientation of the sample with respect to the incoming neutron beam, the profile fitting can be quite good. In other words, the poorer fit in Fig. 5b is believed to be the influence of texture on the diffraction profile and not poor selection of the tetragonal phase structure for fitting sample x = 0.16 (X2B). The small unfitted peak at approximately 2 Aº is suspected to be a magnetic structure peak, but additional work is needed for confirmation.

Figure 6 shows the Heusler austenite ($L2_1$) and the primitive bct martensite (*I4/mmm*) structures of the $Ni_{2+x}Mn_{1-x}Ga$ alloys with axes designated as a, b, and c. In order to relate the measured martensite structure to the parent cubic Heusler $L2_1$ structure, one often multiplies 'a' by √2 and uses the alternative face centered tetragonal (fct) lattice with Z = 4, rather than Z = 2, for the primitive lattice [39]. This cell is represented by the outer fct skeleton with axes a', b', and c'. We thus obtain $a = b = 5.484$ Å, $c = 6.485$ Å (all with a standard deviation of ±0.001 Å) with c/a = 1.182 for the x = 0.16 sample in the martensite state at RT, consistent with other observations on NM martensite in Ni_2MnGa [10, 35, 39].

Crystal structure analyses using selected area diffraction patterns (SADP) and high resolution TEM (HRTEM) confirm the results from the neutron diffraction experiments. The bright field image and HRTEM micrographs of Figure 7a for x = 0.14 shows extensive twinning at multiple length scales in this 7M superstructure, with the minor twins only a few nanometers wide. This type of twinning is characteristic of adaptive martensite, needed to maintain compatibility with the parent face centered cubic $Fm\bar{3}m$ structure of austenite [40, 41]. Fast Fourier transformation (FFT) of the minor twins within a major twin in sample x = 0.14 shows the six superstructure spots characteristic of the 7M modulation. For x = 0.16 alloy, long twins of 10-20 μm widths and stretching across the entire length of the grain are observed in the SEM. In addition, HRTEM micrographs show that nanoscale twinning is also present here, as illustrated in Figure 7b. The diffraction spots from SADP of a twinned location confirms the {110} twin plane of the austenite. Based on the SADP from different orientations, the lattice parameters are determined to be *a=4.24 Å, b=5.44 Å, c=4.21 Å (all with a standard deviation of ±0.01 Å)* for the x = 0.14 sample, and *a=b=3.81 Å* with *c=6.49 Å (all with a standard deviation of ±0.01 Å)* for the primitive bct representation of the x = 0.16 sample. These parameters are close to those deduced from neutron diffraction data.

Figure 8 shows strain vs. T plots from the thermal cycling experiments on sample x = 0.14 under a constant compressive stress of 20 MPa along the central axis of the columnar grains. The strain starts out at zero level at RT and remains constant on heating until about 315 K (42 °C), corresponding to A_s, where it increases rapidly over a temperature interval of approximately 15 K before again becoming constant, this time at a positive strain of ~1.5 %. There is likely some lag in the temperature measurement in these data as the thermocouple was spot welded to the stainless steel foil, rather than directly to the sample (see Fig. 1). The cooling curve is even

more interesting in that there is a ~3 % net decrease in strain during the cooling cycle. The peaks in the curves at approximately 375 K (102 °C) are believed to be artifacts of the cooling arrangement as deduced from a calibration Al-alloy sample. Subsequent thermal cycles generally retraced the 1st cycle data except that it started out at the negative strain level at RT where the first cycle ended. Overall, the plot indicates that the sample experienced a net contraction in length of ~1.5% at RT after cycling. The contraction increased with higher compressive stress, but at 50 MPa the sample cracked after only a few cycles. Clearly this latter stress would be an upper limit for thermomechanical cycling, pending improved methods to eliminate cracking.

The strain results presented for the thermally cycled samples are similar to those that have been observed before in standard NiTi shape memory alloys [17, 18]. For those alloys, it was demonstrated that during the cooling period the martensite variants grew from the prior austenite phase with a preferred crystallographic orientation in the loading direction. In principle, favorable martensite variants can be induced by stress alone below A_s. However, the stress requirements are higher and possibly lead to cracking of the brittle $Ni_{2+x}Mn_{1-x}Ga$ specimens.

Figure 9 shows the effect of thermal cycling under load on the net magnetization at $\mu_0 H$ = 0.1 T, for material x = 0.16 having the tetragonal NM martensite structure. The data below T_C indicates the stress assisted thermally cycled (SATC) sample exhibits a greater magnetization at an applied field of 0.1 T than does the unstressed annealed material. The applied field of $\mu_0 H$ = 0.1 T is not a saturating field, so this does not imply that the saturation magnetization has changed for the SATC x = 0.16 sample. Texture data presented later indicated that there was a preferred orientation of the martensite variants along the loading axis for the SATC sample that likely contributed to the observed increase in magnetization. Figure 9 also shows a subtle increase in the sharpness of the magnetic transition due to thermal cycling, which may be an

indicator of an increased MCE value. Although not shown here, a similar behavior was observed for the x = 0.14 sample with the martensite having the 7M modulated structure. This result suggests that the increase in magnetization for stress assisted thermally cycled samples may be a general result, independent of the crystal structure of the martensite phase.

Figure 10 shows the isothermal magnetization curves for the as-annealed material x = 0.14, where the M vs. $\mu_0 H$ is plotted at different temperatures. The curves are 2 K apart with the green symbols representing data at 320 K. Inflection points in the magnetization are apparent in the 316 K and 314 K isotherms, temperatures which are just above the martensite start temperature of 312 K derived from the DSC measurements (see Table 2). Such inflection points indicate the presence of a magnetic field-induced first order transformation, as from the austenite to the martensite state. These magnetic field induced structural transformations all require $\mu_0 H > 1T$. This is further confirmation that the applied fields used in the M vs. T measurements are not changing the structure during the measurement. As mentioned in the introduction, such field-induced crystallographic phase transformations may be the origin of the "giant" MCE [1, 4]

The magnetic entropy change (ΔS_M), which is a measure of MCE, was determined in this work using the finite difference form of the Maxwell equation that follows from the Gibbs differential [28]; see also the writeup in the Introduction:

$$\Delta S_M(T) \approx \frac{1}{\Delta T}\left[\int_0^{H'} M(T+\Delta T, H)dH - \int_0^{H'} M(T, H)dH\right]$$

Figure 11 illustrates the ΔS_M results obtained for sample x = 0.14 and x = 0.16 before and after stress assisted thermal cycling. The temperatures of maximum MCE for these samples were 315 and 336 K, respectively, and the estimated error on MCE is ±0.5 J/kg-K. The MCE results are given for magnetic field changes of 2, 5, and 7 T, where it may be noted that 2 T is within the capability of permanent magnets/electromagnets. The bar chart shows that the x = 0.16 sample,

which had near coincidence of the structural and magnetic transformations, had a greater MCE values than the x = 0.14 sample. Second, both samples had MCE values comparable to or higher than that for Gd and $Gd_5(SiGe)_2$, both of which exhibit their large values at RT [1]. At 2T our data for the x =0.16 sample are similar to values reported for MnFe based alloys [42] that are viewed with strong commercial interest. Finally, both the x = 0.16 and x = 0.14 samples exhibited greater MCE values after the stress assisted thermal cycling. For example, in the case of x = 0.16, the MCE value increased by approximately 84 % in a field change of 2 T compared to the uncycled sample.

In order to find possible mechanisms for the observed increases in MCE following thermal cycling under load, the texture of the samples was evaluated at RT when they were in the martensite phase. As mentioned in the introduction, the rationale for conducting the thermal cycling (under load) experiments was to predispose the martensite platelets to take on a favored orientation, such that the easy magnetization axis was along the direction of the applied field. Thus, on transitioning from the paramagnetic to the ferromagnetic state during the phase transformation under an applied magnetic field, there would be a larger magnetization change; i.e., a larger magnetic entropy decrease.

Texture measurements using neutron diffraction were conducted at RT on a different sample, still with a composition of x = 0.16 (X5D, see Tables 1 and 2) in the uncycled and thermally cycled states. Notably, this material had an identical DSC trace to that of the x = 0.16 material previously discussed (X2B), and also exhibited a NM tetragonal structure with similar lattice parameters. The MCE has not been determined for this material yet, but its texture should be comparable to that of the previous x = 0.16 (X2B) sample.

Figure 12 shows pole figure plots for sample x = 0.16 (X5D) in the uncycled and thermally cycled conditions. In this figure, the columnar direction of the cast button is at the center of the pole figures, while the points on the circumference represent directions that are orthogonal to the columnar axis and are not anticipated to possess any preferential texture. The upper row of pole figures in Figure 12 shows that there is approximately 5-6 multiples of random distribution (MRD) of the (110) and (002) poles for the initial uncycled material along the columnar growth direction. It may be recalled that the columnar growth direction was also the direction along which the magnetic field was applied during magnetic characterization of the samples. The overall texture index was 9.2±2, which indicates a fairly strong preferred orientation for the arc melted button in the as-annealed state. The top row of pole figures for the uncycled state shows almost similar intensity of (110) and (002) poles distributed around the circumference (perpendicular to the columnar growth direction) and at the center (parallel to the columnar growth direction).

The bottom row of pole figures for the x = 0.16 SATC sample demonstrates two important facts. First, there is a far greater population of tetragonal martensite crystals with (110) poles along the center, which represents the columnar growth direction. The overall texture index is now 19±2, a high value representing almost single crystal orientation along the columnar axis. Second, this (110) population increase is accompanied with (002) poles being depleted from the loading axis (center) and enhanced perpendicular to the loading axis. These population changes begin to make sense by referring to Figure 6, where one may note that the two poles are orthogonal to each other and indeed are related by twinning across the {112} twin plane of the tetragonal structure [43]. This realignment of martensite poles occurred due to thermal cycling

under load, and so is a crystallographic reason that may help explain the superior MCE performance of the cycled over the uncycled x = 0.16 material.

Although not shown in Figure 12, the primitive bct based crystal parameters were $a = b = 3.896$ Å, $c = 6.484$ Å, and c/a = 1.664 for the uncycled x = 0.16 material. This changed slightly to $a = b = 3.811$ Å, $c = 6.342$ Å, and c/a = 1.664 for the stress assisted thermally cycled material. It therefore follows that there was a slight contraction of the d-spacing of the (110) planes following thermal cycling, part of which may be responsible for the net contraction of the sample along the columnar growth direction after thermal cycling. A second and more important reason for the contraction is believed to be the replacement of martensite crystals with a longer [002] c-axis along the columnar growth direction by a shorter [110] axis.

4. Discussion

Here, we investigated polycrystalline alloys in the $Ni_{2+x}Mn_{1-x}Ga$ family with the idea of enhancing the MCE through simultaneous structural and magnetic transformations close to room temperature and creation of favorable texture to facilitate magnetic alignment along a preferred crystallographic direction. Although a constant Ga content necessarily restricted the search domain, this research does provide insight toward the development of a systematic methodology for finding new alloys. For example, Figures 3 and 4 show that DSC experiments may be useful for screening Heusler alloys for compositions that exhibit close coupling between the structural and magnetic transformations temperatures.

The phase diagram in Figure 4 shows that while T_C does not change much with composition, the structural transformation temperature does increase monotonically with the Ni atomic percentage (equivalently the e/a ratio), with a crossover around 353 K between x = 0.16

and 0.19 (e/a of 7.61 to 7.64), see Table 1). Indeed, the phase diagram suggests that the alloy with nominal x = 0.19 may also provide good MCE values, but the alloy has thus far not been characterized. Furthermore, the diagram shows that in order to move the simultaneous transformations from 335 K to 298 K (RT), the T_C would need to be reduced through alloy modification. In alloys where Ga is substituted with Sn or In, such decreases in T_C are observed although in those cases an inverse MCE is observed [44, 45].

It is also interesting to note that the entropy of transformation obtained from the DSC curves reached a maximum at x = 0.16 (Table 2). This high entropy of transformation may be a result of changes in the configurational entropy of spins associated with the simultaneous magnetic transformation for this alloy composition (see Figure 4) as well as possible coupling between the magnetic and vibrational degrees of freedom [46]. The data in Table 2 also indicates that the entropy for this material increased slightly with stress assisted thermal cycling although it decreased for the x=0.14 sample. These differences may arise from changes in the magnetic structures because of observed small changes in lattice parameters following SATC; estimations of magnetic structure changes based on neutron diffraction data remain part of our future work. Table 2 shows that the structural transformation temperatures (such as M_s, A_s..) barely changed with SATC, and Figure 9 illustrates that there also was a negligible change in the magnetic transformation temperature. Thus, the DSC and magnetization data do not give any reason to suspect that SATC led to any major changes in the structural and magnetic states of the material and therefore the measured MCE changes using Maxwell's relations is a good representation of the material in the as-annealed and SATC states. Indeed, the higher magnetization at low fields observed in Figure 9 for the SATC sample is a reflection of the magnetic easy axis alignment of the ferromagnetic martensite phase along the magnetic field direction.

An important goal of this work was to evaluate alloys of polycrystalline morphology instead of the single crystals that are common in magnetic shape memory applications. The benefits of polycrystalline samples are cost, effort, reliability, and scalability, all of which are important in current manufacturing technology. One way to overcome the deficiency of polycrystals is texturing, which was attempted herein.

The MCE measurements show that the ΔS_M is higher for x = 0.16 alloy vs. the x = 0.14 alloy, where the former exhibited a much better overlap of structural and magnetic phase transformations. It is also important to note that x = 0.16 had a NM structure whereas x = 0.14 had a 7M structure. The latter structure is generally known to possess greater mobility of martensite variants, according to the magnetic shape memory alloy literature [10, 47]. Our current observations therefore suggest that overlap of transformation peaks is more important in MCE performance than the relevant structure (modulated vs. non-modulated).

The magnetocaloric data from the SATC samples were more than 50% higher than the non-cycled samples, representing an enhanced magnetostructural coupling (see Figure 11). Figure 12 shows that the enhanced MCE was accompanied with a strong increase in preferred orientation of (110) poles along the mechanical loading axis, which was also the columnar growth direction and subsequent magnetization axis. In order to understand this correlation, it is important to analyze the crystallographic and texture results.

Figure 12 indicates that the strong (110) preferred orientation along the loading axis came at the expense of (002) poles that were initially along that axis. Figure 6 shows that these orthogonal poles are related by twin across the favored (112) twin plane (ABC plane). Thus, the presence of compressive load during thermal cycling is likely to have led to twinning across the (112) twin plane, whereby variants with (002) poles with larger d-spacing were converted to

(110) poles with smaller d-spacing along the loading axis. As suggested earlier, thermal cycling aided the twinning process by reducing the stress needed for deformation twinning [26, 27].

Figure 6 also shows that the (110) pole represents the diagonal direction that connects Mn atoms at the corners of the tetragonal lattice. In order to relate this direction to the easy magnetization axis that is referenced in the literature on MSMA, it is useful to convert the *I4/mmm* tetragonal structure to the alternate fct designation of the parent austenite cell ($Fm\bar{3}m$). This is depicted in Figure 5b by the outer rectangular green colored lines. Here, the bct (110) pole is coincident with the a-axis of the fct structure, while the c-axis directions remain coincident. In addition, the twin plane becomes the standard (101) plane of the fct lattice with c/a = 1.18 > 1, which is in agreement with the description of the NM martensite structure in the MSMA literature [10]. Furthermore, it has been observed that the easy magnetization axis in the NM structure (with c/a >1) is the shorter a-axis, in contrast to the 7M structure (with c/a <1) where the c-axis is the easy magnetization axis [11]. It therefore follows that the strong preferred orientation of (110) poles in the bct lattice (equivalently the (100) pole in the fct lattice) was responsible for the greater magnetization in the thermally cycled material, as observed in Figure 9. In short, the textural change can explain the observed permanent decrease in specimen height as well as the enhanced magnetization following stress assisted thermal cycling. The latter also explains the 84% increase in MCE with a field change of 2 T in the polycrystalline material following thermomechanical cycling, since the texture index of 19.2 for the martensite phase is considered high. As shown in Figure 11, the MCE data following cycling competes very well with some of the best materials in the literature.

In summary, the results suggest that it may be possible to enhance the MCE performance of current Heusler based polycrystalline materials by predisposing the orientation of the

martensite variants. While the influence of twin mobility brought about by thermal cycling under load cannot be ruled out at present, verification of the mechanism would require accurate flow stress measurements of polycrystalline samples with and without SATC. In the absence of quantitative verification as well as evaluation of possible changes to the magnetic structure due to cycling, a texture based mechanism appears adequate for explaining enhanced MCE due to stress assisted thermal cycling. Finally, it may be recalled that stress assisted thermal cycling was conducted to take advantage of the low shear modulus at the transformation temperature. Thereby, stresses could be kept low to prevent possible specimen cracking. The current results suggest that the procedure works and may be adapted to other similar magnetocaloric materials.

5. Conclusions

Alloys belonging to the $Ni_{2+x}Mn_{1-x}Ga$ Heusler family were evaluated, resulting in the following:

(1) DSC measurements may be useful to screen alloys for near coincidence of structural and magnetic transformation temperatures. A preliminary phase diagram based on observed first (structural) and second order (magnetic) transformation has been demonstrated.

(2) Magnetic measurements show that the x = 0.16 material with coinciding structural and magnetic transformations was the composition in our samples with the highest MCE, consistent with other observations in the literature.

(3) The results show that there was an 84% increase in ΔS_M with a field change of 2 T due to thermal cycling under a constant compressive load, from below the martensite start temperature to above the austentite finish temperature.

(4) A key finding of the research is that favorable martensite alignment brought about by stress assisted thermal cycling was a mechanism contributing to the large MCE increase.

6. Acknowledgments

Funding for this research came through Cooperative Program Agreement W911NF-11-2-0036 with the Army through the Army Research Laboratories, Proving Grounds, Maryland. The authors thank S. Claggett for help with the sectioning of the magnetometry samples. The authors also thank Dr. A. Haq of the Oak Ridge National Laboratory for the neutron diffractometer experiments on POWGEN, and LANSCE, Los Alamos National Laboratory for conducting the texture measurements on the HIPPO neutron diffractometer. The SNS site at Oak Ridge National Laboratory was supported by DoE BES under DE-AC05-00OR22725, and LANSCE by DoE BES under contract W-7405-ENG-36. BSM would like to thank EPFL, in Lausanne, Switzerland, for hosting him at the LMM in the Institute of Materials, during the review portion of this paper.

[DISCLAIMER] The use of manufacturer names in this paper is only for the purpose of properly describing the experimental conditions and does not imply an endorsement by the authors or by their organizations.

REFERENCES

[1] Pecharsky, V. K., and Gschneidner, K. A., 1997, "Giant Magnetocaloric Effect in Gd-5(Si2ge2)," Physical Review Letters, 78(23), pp. 4494-4497.
[2] Planes, A., Manosa, L., and Acet, M., 2009, "Magnetocaloric Effect and Its Relation to Shape-Memory Properties in Ferromagnetic Heusler Alloys," Journal of Physics-Condensed Matter, 21(23), pp. 29.
[3] Provenzano, V., Shapiro, A. J., and Shull, R. D., 2005, "Reduction of Hysteresis Losses in the Magnetic Refrigerant Gd5ge2si2 by the Addition of Iron," Nature, 429(pp. 853-857.
[4] Pecharsky, V. K., Holm, A. P., Gschneidner, K. A., and Rink, R., 2003, "Massive Magnetic-Field-Induced Structural Transformation in Gd5ge4 and the Nature of the Giant Magnetocaloric Effect," Physical Review Letters, 91(19), pp. 4.

[5] Gschneidner, K. A., Mudryk, Y., and Pecharsky, V. K., 2012, "On the Nature of the Magnetocaloric Effect of the First-Order Magnetostructural Transition," Scripta Materialia, 67(6), pp. 572-577.
[6] Gschneidner, K. A., and Pecharsky, V. K., 2008, "Thirty Years of near Room Temperature Magnetic Cooling: Where We Are Today and Future Prospects," International Journal of Refrigeration, 31(6), pp. 945-961.
[7] Franco, V., Blazquez, J. S., Ingale, B., and Conde, A., 2012, Annual Review of Materials Research, Vol 42.
[8] Takeuchi, I., Famodu, O. O., Read, J. C., Aronova, M. A., Chang, K. S., Craciunescu, C., Lofland, S. E., Wuttig, M., Wellstood, F. C., Knauss, L., and Orozco, A., 2003, "Identification of Novel Compositions of Ferromagnetic Shape-Memory Alloys Using Composition Spreads," Nature Materials, 2(3), pp. 180-184.
[9] Webster, P. J., Ziebeck, K. R. A., Town, S. L., and Peak, M. S., 1984, "Magnetic Order and Phase-Transformation in Ni2mnga," Philosophical Magazine B-Physics of Condensed Matter Statistical Mechanics Electronic Optical and Magnetic Properties, 49(3), pp. 295-310.
[10] Lanska, N., Soderberg, O., Sozinov, A., Ge, Y., Ullakko, K., and Lindroos, V. K., 2004, "Composition and Temperature Dependence of the Crystal Structure of Ni-Mn-Ga Alloys," Journal of Applied Physics, 95(12), pp. 8074-8078.
[11] Sozinov, A., Likhachev, A. A., and Ullakko, K., 2001, Smart Structures and Materials 2001: Active Materials: Behavior and Mechanics, SPIE-Int Soc Optical Engineering, Bellingham.
[12] Ullakko, K., Huang, J. K., Kantner, C., Ohandley, R. C., and Kokorin, V. V., 1996, "Large Magnetic-Field-Induced Strains in Ni2mnga Single Crystals," Applied Physics Letters, 69(13), pp. 1966-1968.
[13] Wayman, C. M., 1992, "Shape Memory and Related Phenomena," Progress in Materials Science, 36(pp. 203-224.
[14] Wayman, C. M., 1983, Physical Metallurgy, 3rd Edition, Elsevier, Chap. 14.
[15] Otsuka, K., and Ren, X., 2005, "Physical Metallurgy of Ti-Ni-Based Shape Memory Alloys," Progress in Materials Science, 50(5), pp. 511-678.
[16] Sehitoglu, H., Hamilton, R., Canadinc, D., Zhang, X., Gall, K., Karaman, I., Chumlyakov, Y., and Maier, H., 2003, "Detwinning in Niti Alloys," Metallurgical and Materials Transactions A, 34(pp. 5-13.
[17] Ye, B., Majumdar, B. S., and Dutta, I., 2007, "Texture Memory and Strain-Texture Mapping in a Niti Shape Memory Alloy," Applied Physics Letters, 91(6), pp. 061918.
[18] Ye, B., Majumdar, B. S., and Dutta, I., 2009, "Texture Development and Strain Hysteresis in a Niti Shape-Memory Alloy During Thermal Cycling under Load," Acta Materialia, 57(8), pp. 2403-2417.
[19] Pecharsky, V. K., and Gschneidner, K. A., 1999, "Magnetocaloric Effect from Indirect Measurements: Magnetization and Heat Capacity," Journal of Applied Physics, 86(1), pp. 565-575.
[20] Caron, L., Ou, Z. Q., Nguyen, T. T., Thanh, D. T. C., Tegus, O., and Bruck, E., 2009, "On the Determination of the Magnetic Entropy Change in Materials with First-Order Transitions," Journal of Magnetism and Magnetic Materials, 321(21), pp. 3559-3566.
[21] Pareti, L., Solzi, M., Albertini, F., and Paoluzi, A., 2003, "Giant Entropy Change at the Co-Occurrence of Structural and Magnetic Transitions in the Ni2.19mn0.81ga Heusler Alloy," European Physical Journal B, 32(3), pp. 303-307.

[22] Mandal, K., Pal, D., Scheerbaum, N., Lyubina, J., and Gutfleisch, O., 2008, "Magnetocaloric Effect in Ni-Mn-Ga Alloys," IEEE Transactions on Magnetics, 44(11), pp. 2993-2996.
[23] Pasquale, M., Sasso, C. P., Lewis, L. H., Giudici, L., Lograsso, T., and Schlagel, D., 2005, "Magnetostructural Transition and Magnetocaloric Effect in Ni55mn20ga25 Single Crystals," Physical Review B, 72(9), pp. 5.
[24] Sasso, C. P., Pasquale, M., Giudici, L., Besseghini, S., Villa, E., Lewis, L. H., Lograsso, T. A., and Schlagel, D. L., 2006, "Magnetostructural Transitions and Adiabatic Temperature Variation in Polycrystal and Single-Crystal Ni2mnga Alloys," Journal of Applied Physics, 99(8), pp. 3.
[25] Brill, T. M., Mittelbach, S., Assmus, W., Mullner, M., and Luthi, B., 1991, "Elastic Properties of Niti," J. Phys. Condens. Matter 3(pp. 9621-9627.
[26] Manosa, L., Gonzalezcomas, A., Obrado, E., Planes, A., Chernenko, V. A., Kokorin, V. V., and Cesari, E., 1997, "Anomalies Related to the Ta(2)-Phonon-Mode Condensation in the Heusler Ni2mnga Alloy," Physical Review B, 55(17), pp. 11068-11071.
[27] Manosa, L., Planes, A., Zarestky, J., Lograsso, T., Schlagel, D. L., and Stassis, C., 2001, "Phonon Softening in Ni-Mn-Ga Alloys," Physical Review B, 64(2), pp. 024305.
[28] Giri, A. K., Paterson, B. A., Mcleod, M. V., Dennis, C. L., Majumdar, B. S., Cho, K. C., and Shull, R. D., 2013, "Effect of Crystallographic Alignment on the Magnetocaloric Effect in Alloys near the Ni2mnga Stoichiometry," Journal of Applied Physics, 17A907(17).
[29] Larson, A. C., and Von Dreele, R. B., 2004, "General Structure Analysis System (Gsas)," Los Alamos National Laboratory.
[30] Wenk, H. R., Lutterotti, L., and Vogel, S., 2003, "Texture Analysis with the New Hippo Tof Diffractometer," Nuclear Instruments and Methods in Physics Research Section A: Accelerators, Spectrometers, Detectors and Associated Equipment, 515(3), pp. 575-588.
[31] Vogel, S. C., Hartig, C., Lutterotti, L., Von Dreele, R. B., Wenk, H.-R., and Williams, D. J., 2004, "Texture Measurements Using the New Neutron Diffractometer Hippo and Their Analysis Using the Rietveld Method," Powder Diffraction, 19(1), pp. 65-68.
[32] Lutterotti, L., 2010, "Total Pattern Fitting for the Combined Size-Strain-Stress-Texture Determination in Thin Film Diffraction," Nuclear Instruments & Methods in Physics Research Section B-Beam Interactions with Materials and Atoms, 268(3-4), pp. 334-340.
[33] Lutterotti, L., Matthies, S., Wenk, H. R., Schultz, A. S., and Richardson, J. W., 1997, "Combined Texture and Structure Analysis of Deformed Limestone from Time-of-Flight Neutron Diffraction Spectra," Journal of Applied Physics, 81(2), pp. 594-600.
[34] Wenk, H. R., Lutterotti, L., and Vogel, S. C., 2010, "Rietveld Texture Analysis from Tof Neutron Diffraction Data," Powder Diffraction, 25(3), pp. 283-296.
[35] Sozinov, A., Likhachev, A. A., and Ullakko, K., 2002, "Crystal Structures and Magnetic Anisotropy Properties of Ni-Mn-Ga Martensitic Phases with Giant Magnetic-Field-Induced Strain," Magnetics, IEEE Transactions on, 38(5), pp. 2814-2816.
[36] Straka, L., Heczko, O., and Hanninen, H., 2008, "Activation of Magnetic Shape Memory Effect in Ni-Mn-Ga Alloys by Mechanical and Magnetic Treatment," Acta Materialia, 56(19), pp. 5492-5499.
[37] Liu, Y. N., Liu, Y., and Van Humbeeck, J., 1998, "Two-Way Shape Memory Effect Developed by Martensite Deformation in Niti," Acta Materialia, 47(1), pp. 199-209.

[38] Simon, T., Kroger, A., Somsen, C., Dlouhy, A., and Eggeler, G., 2010, "On the Multiplication of Dislocations During Martensitic Transformations in Niti Shape Memory Alloys," Acta Materialia, 58(5), pp. 1850-1860.
[39] Banik, S., Ranjan, R., Chakrabarti, A., Bhardwaj, S., Lalla, N. P., Awasthi, A. M., Sathe, V., Phase, D. M., Mukhopadhyay, P. K., Pandey, D., and Barman, S. R., 2007, "Structural Studies of Ni2+Xmn1-Xga by Powder X-Ray Diffraction and Total Energy Calculations," Physical Review B, 75(10).
[40] Khachaturyan, A. G., Shapiro, S. M., and Semenovskaya, S., 1991, "Adaptive Phase Formation in Martensitic Transformation," Physical Review B, 43(13), pp. 10832.
[41] Roytburd, A. L., and Slutsker, J., 2001, "Deformation of Adaptive Materials. Part Iii: Deformation of Crystals with Polytwin Product Phases," Journal of the Mechanics and Physics of Solids, 49(8), pp. 1795-1822.
[42] Yibole, H., Guillou, F., Zhang, L., Van Dijk, N. H., and Bruck, E., 2014, "Direct Measurement of the Magnetocaloric Effect in Mnfe(P,X) (X = as, Ge, Si) Materials," Journal of Physics D-Applied Physics, 47(7), pp. 9.
[43] Christian, J. W., and Mahajan, S., 1995, "Deformation Twinning," Progress in Materials Science, 39(1-2), pp. 1-157.
[44] Krenke, T., Acet, M., Wassermann, E. F., Moya, X., Manosa, L., and Planes, A., 2006, "Ferromagnetism in the Austenitic and Martensitic States of Ni-Mn-in Alloys," Physical Review B, 73(17), pp. 174413.
[45] Krenke, T., Duman, E., Acet, M., Wassermann, E. F., Moya, X., Manosa, L., and Planes, A., 2005, "Inverse Magnetocaloric Effect in Ferromagnetic Ni-Mn-Sn Alloys," Nature Materials, 4(6), pp. 450-454.
[46] Fultz, B., 2010, "Vibrational Thermodynamics of Materials," Progress in Materials Science, 55(4), pp. 247-352.
[47] Sozinov, A., Likhachev, A. A., Lanska, N., and Ullakko, K., 2002, "Giant Magnetic-Field-Induced Strain in Nimnga Seven-Layered Martensitic Phase," Applied Physics Letters, 80(10), pp. 1746-1748.

List of Tables

List of Figures

Figure 4. A phase diagram based on DSC and T_c data. The open circles represent T_c values whereas the solid diamonds represent temperatures at inflection points, characteristic of second order transformation, in the DSC plots.

Figure 5. Results of Rietveld fitting of neutron diffraction data of samples from POWGEN SNS using GSAS code. (a) Data for uncycled sample x=0.14 which exhibits a 7M modulated martensite structure; (b) uncycled sample x=0.16 that exhibits a non-modulated martensite structure.

Figure 6. Schematics illustrating (a) the crystal structures of the parent cubic ($Fm\bar{3}m$) austenite, and, (b) the primitive bct structure (*I4/mmm*) of martensite for alloy x=0.16 (X2B and X5D). The alternate fct ($Fm\bar{3}m$) representation of the bct martensite is shown by the outer rectangular lines colored green in (b).

Figure 7. (a) Bright field and HRTEM image of sample X2A, and corresponding SADP and FFT, illustrating the six superlattice spots between major reflections characteristic of 7M modulated structure. (b) HRTEM image of sample X2B showing a non-modulated structure. The zone axis is $[1\,\bar{3}\,1]$ and the twinning plane is (202) austenite.

Figure 8. Strain versus temperature during the first four thermal cycles under 20 MPa compressive stress for sample x = 0.14 (X2A). The large strain excursions coincide closely with the transformation temperature indicating they are associated with martensite to austenite transformations. The sample is net about 1.5% shorter at RT after the thermal cycling under load.

Figure 9. Magnetization data at low constant magnetic field $\mu_0 H$ = 0.1T, for material x=0.16 in the as-heat treated (lower curve) state and following thermally cycling at a constant compressive stress (upper curve). Error on magnetization is

Figure 10. Isothermal M versus H plot for material x=0.14 before thermal cycling showing sharp magnetization changes at finite magnetic fields around 318 K. This is indicative of field induced structural transformation. Each curve is spaced from the adjacent one by 2 K.

Figure 11. Magnetic entropy change for materials x =0.14 (X2A) and x = 0.16 (X2B) for magnetic field changes $\Delta(\mu_o H)$ = 2, 5 and 7T. Error on MCE is estimated to be ±0.5 J/kg-K. Data for uncycled and thermally cycled samples are shown, being

designated as Before and After, respectively. Also illustrated in this figure are data for Gd and $Gd_5(Si_2Ge)_2$[1], two of the important materials in magnetic refrigeration technology.

Figure 12. Pole figure plots for x=0.16 (X5D) in the uncycled (top row) and the stress assisted thermally cycled (bottom row) states. The texture indices were 9.2 and 19, respectively, for these two conditions. In these plots, the columnar direction of the cast buttons is at the center of each pole figure while the circumference refers to directions perpendicular to the columnar axis. The magnetic field was also applied along the columnar axis.

Supplementary Figures

Figure S1. Diffraction profile for x = 0.16 sample obtained on the HIPPO diffractometer for detector bank oriented at 40 degrees; the blue points refer to the data and the red line corresponds to the fitted profile. Fitting was done using the MAUD program which internally utilizes Rietveld refinement. The locations of the tetragonal peaks are also shown in the plot.

FIGURES

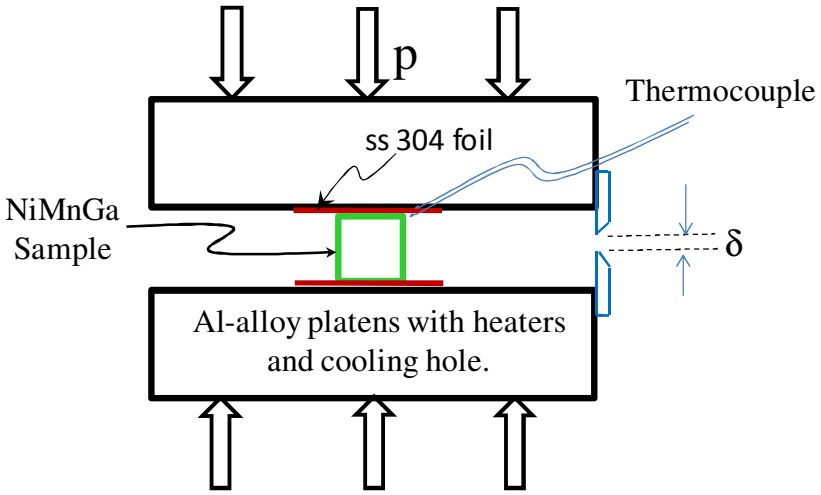

Figure 1

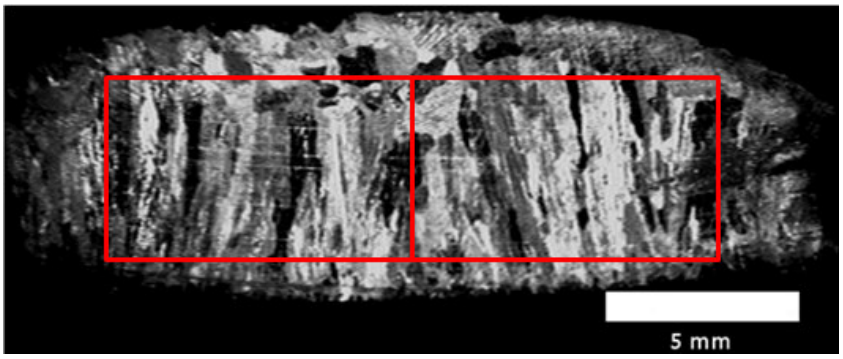

Figure 2

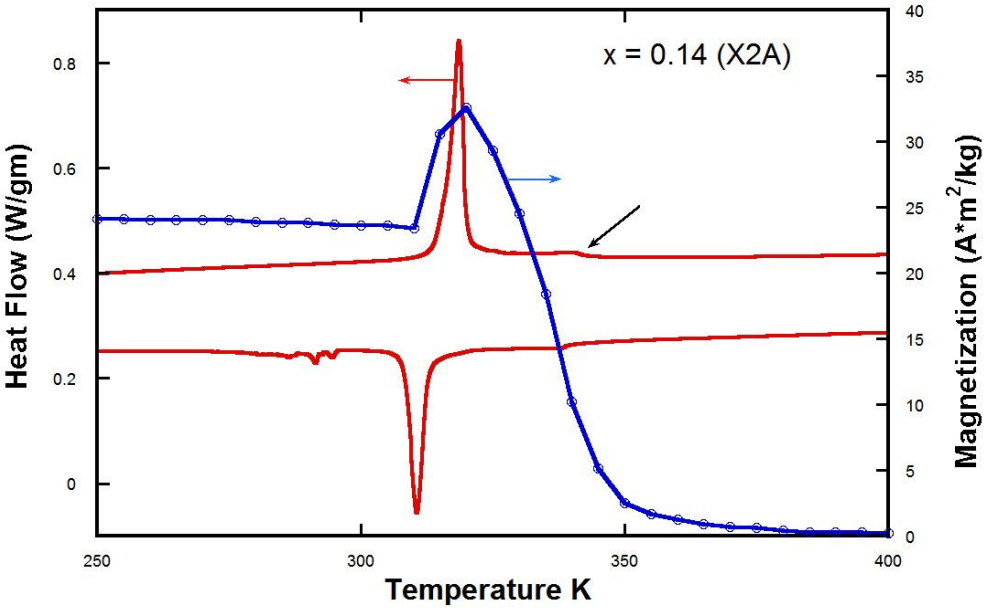
x = 0.14 (X2A)
Heat Flow (W/gm)
Magnetization (A*m^2/kg)
Temperature K
0
0.2
0.4
0.6
0.8
0
5
10
15
20
25
30
35
40
250
300
350
400

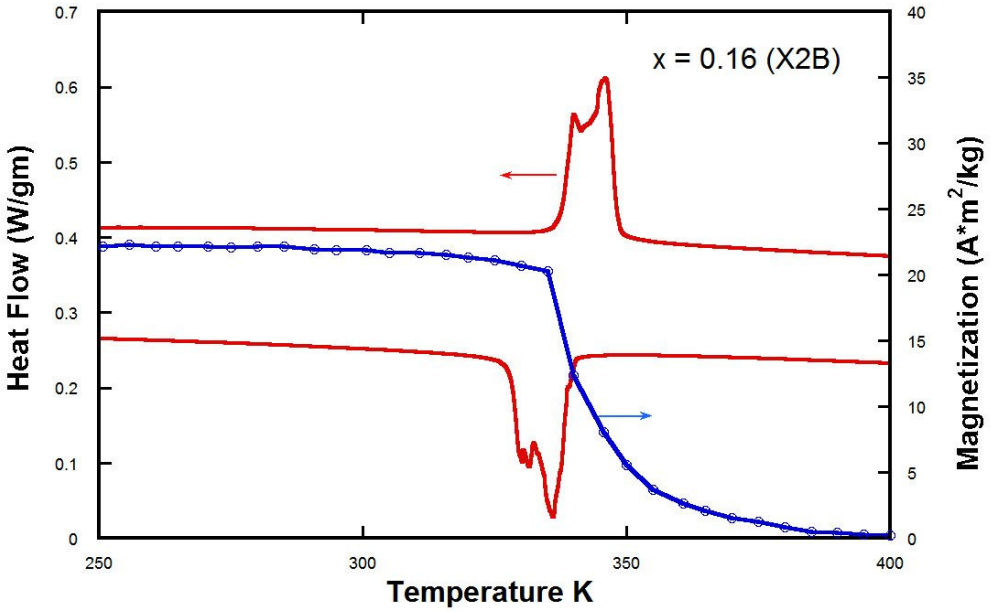
x = 0.16 (X2B)
Heat Flow (W/gm)
Magnetization (A*m^2/kg)
Temperature K
0
0.1
0.2
0.3
0.4
0.5
0.6
0.7
0
5
10
15
20
25
30
35
40
250
300
350
400

Figure 3b

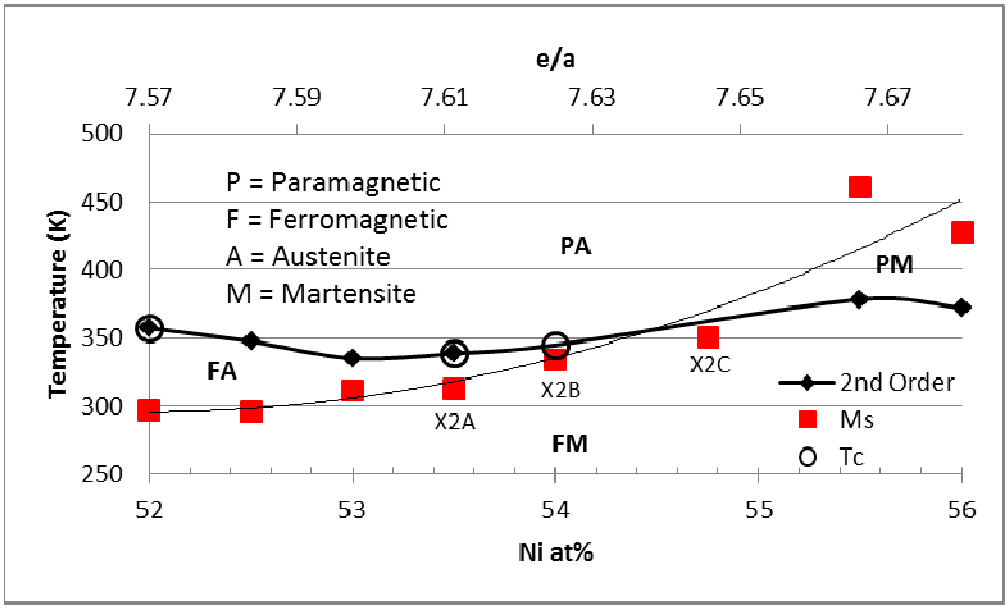

Figure 4

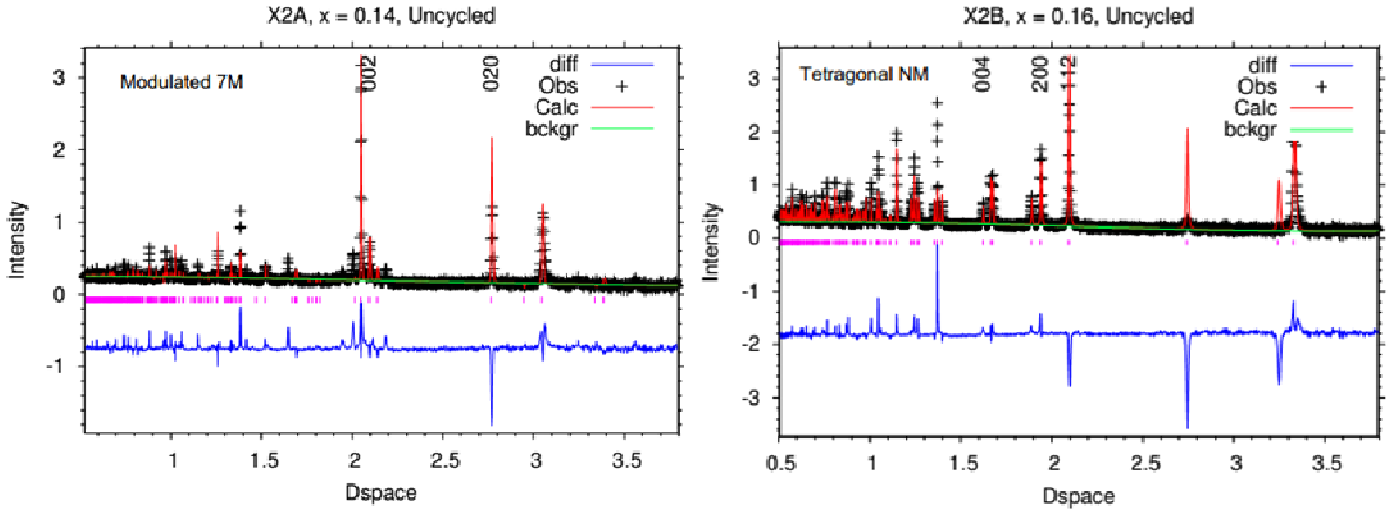

Figure 5

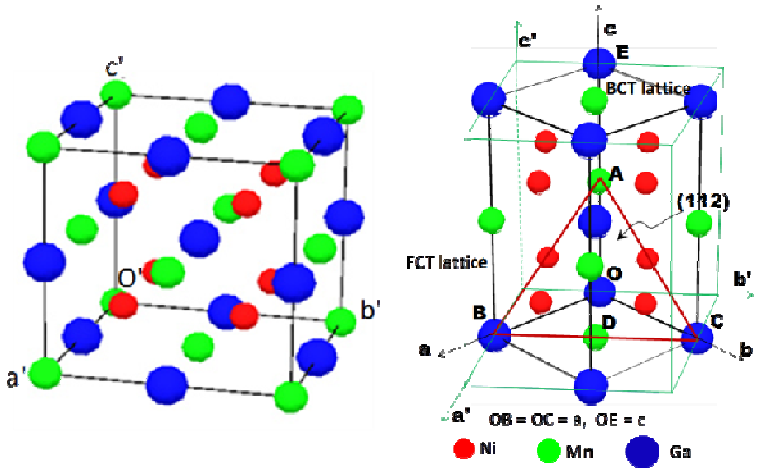
c'
O'
b'
a'
c
c'
E
BCT lattice
A
(112)
FCT lattice
O
b'
B
D
C
a
b
a'
OB = OC = a, OE = c
Ni
Mn
Ga

Figure 6

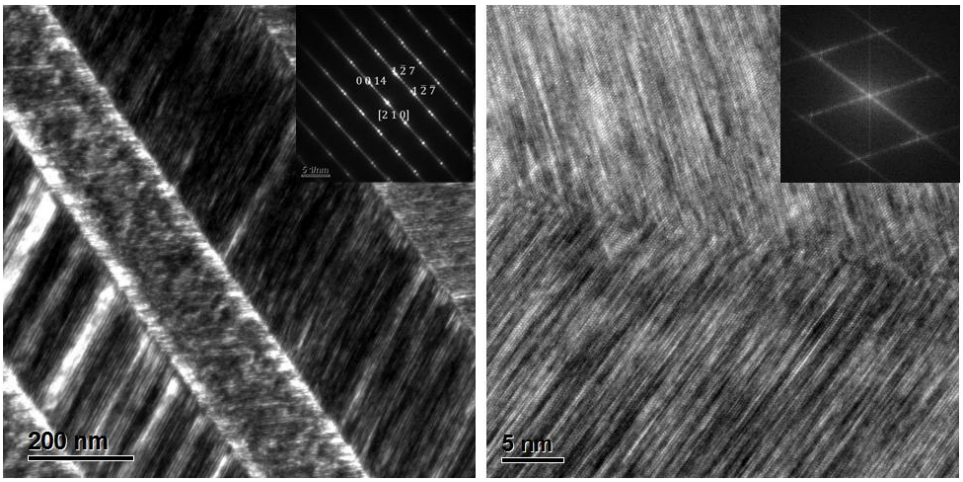

Figure 7a (x=0.14 7M modulated)

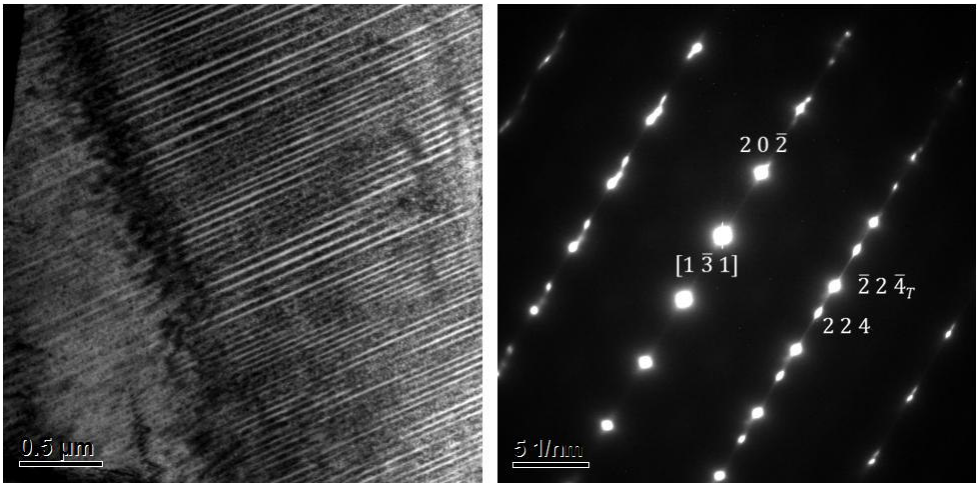

Figure 7b (x=0.16, NM)

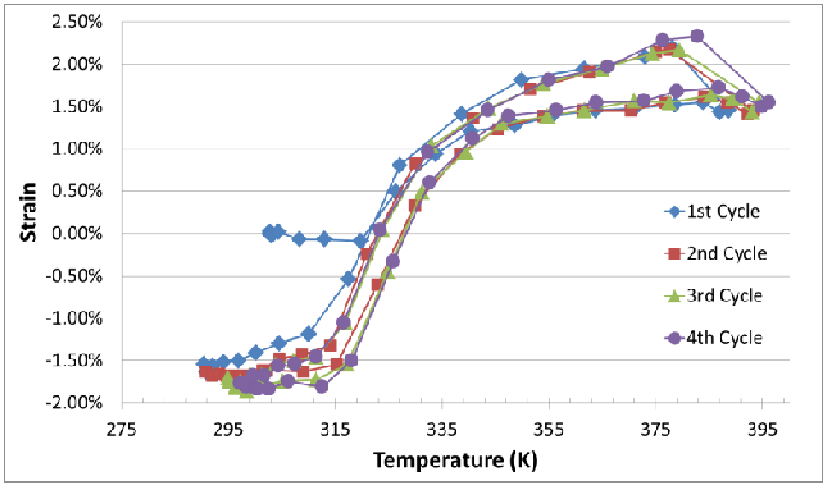
2.50%
2.00%
1.50%
1.00%
0.50%
0.00%
-0.50%
-1.00%
-1.50%
-2.00%
Strain
275
295
315
335
355
375
395
Temperature (K)
1st Cycle
2nd Cycle
3rd Cycle
4th Cycle

Figure 8

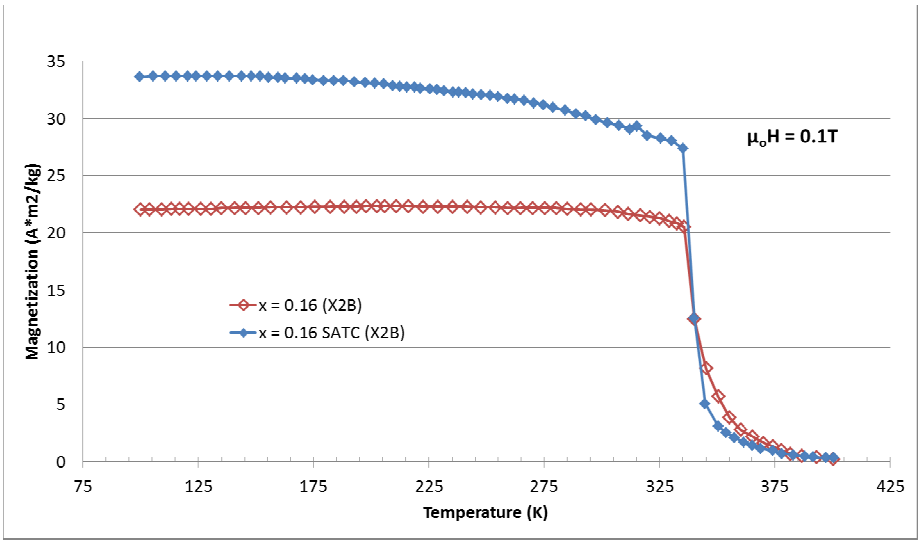
35
30
25
20
15
10
5
0
75
125
175
225
275
325
375
425
Magnetization (A*m2/kg)
Temperature (K)
μ0H = 0.1T
x = 0.16 (X2B)
x = 0.16 SATC (X2B)

Figure 9

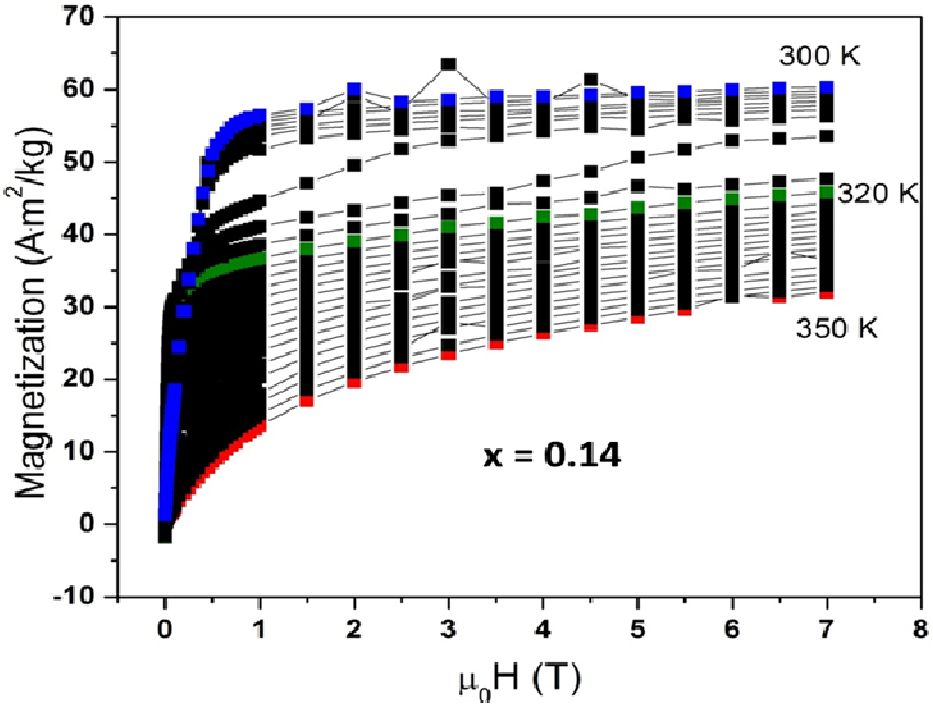
300 K
320 K
350 K
x = 0.14
Magnetization (A·m²/kg)
μ0H (T)
70
60
50
40
30
20
10
0
-10
0
1
2
3
4
5
6
7
8

Figure 10

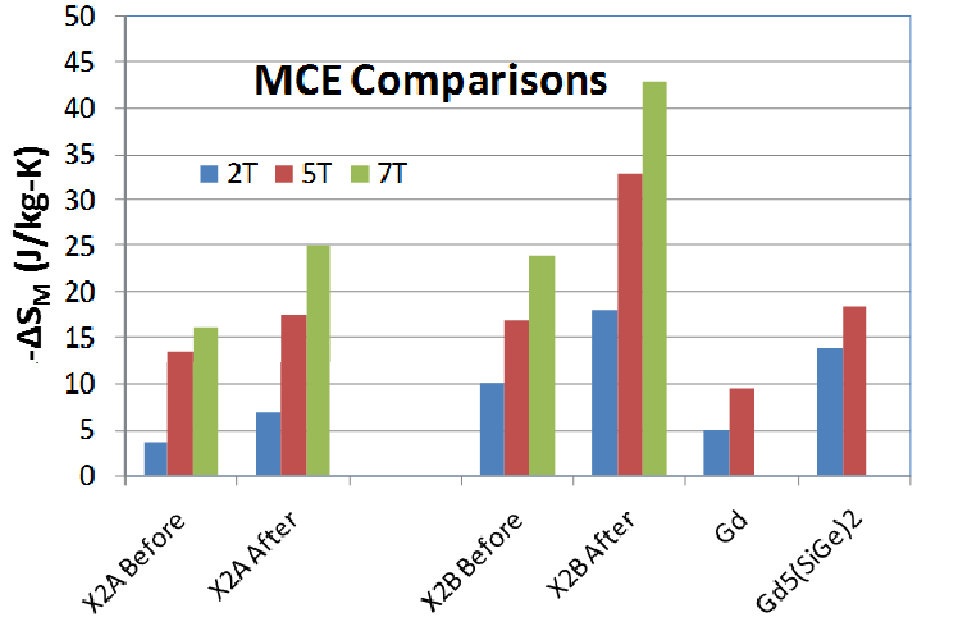
MCE Comparisons
2T
5T
7T
-ΔSM (J/kg-K)
50
45
40
35
30
25
20
15
10
5
0
X2A Before
X2A After
X2B Before
X2B After
Gd
Gd5(SiGe)2

Figure 11

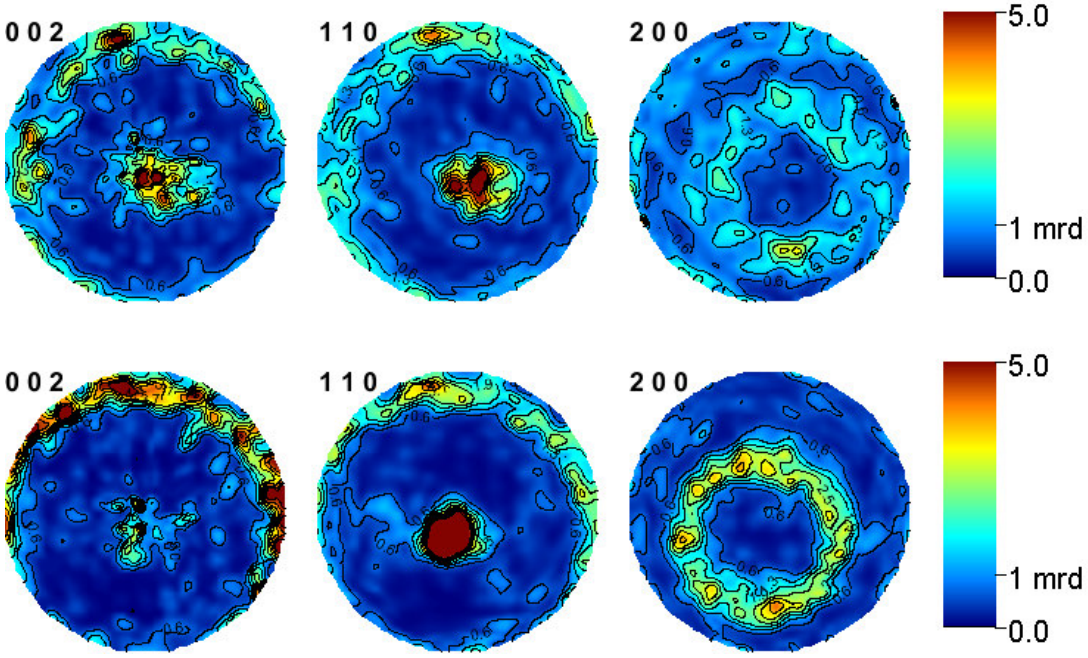

Figure 12

Table 1. Composition of the alloys utilized in this investigation.

		Atomic Ratio				
Sample	**x**	**Ni**	**Mn**	**Ga**	**e/a Starting**	**e/a Actual**
X5A	0.08	2.08	0.92	1.00	7.57	-
X5B	0.10	2.10	0.90	1.00	7.58	-
X5C	0.12	2.12	0.88	1.00	7.59	-
X2A	**0.14**	**2.14 (2.12)**	**0.86 (0.85)**	**1.00 (1.03)**	**7.61**	**7.56**
X2B	**0.16**	**2.16 (2.16)**	**0.84 (0.82)**	**1.00 (1.03)**	**7.62**	**7.59**
X5D	0.16	2.14 (2.17)	0.86 (0.83)	1.00 (1.00)	7.61	7.63
X2C	0.19	2.19 (2.18)	0.81 (0.78)	1.00 (1.04)	7.64	7.60
X2D	0.22	2.22 (2.21)	0.78 (0.77)	1.00 (1.02)	7.67	7.63
X2E	0.24	2.24 (2.24)	0.76 (0.74)	1.00 (1.02)	7.68	7.66

$$\frac{e}{a} = \frac{10.Ni_{at\%} + 7.Mn_{at\%} + 3Ga_{at\%}}{Ni_{at\%} + Mn_{at\%} + Ga_{at\%}}$$

Table 2. Results of DSC measurements for the alloys studied. A_s is the austentite start, A_f is the austenite finish, M_s is the martensite start, and M_f is the martensite finish temperature, and enthalpy and average entropy (enthalpy divided by the average of M_s and M_f) refer to changes associated with the structural transformation obtained from the cooling portion of the DSC data. The Curie temperature is also included in the last column.

			All in Degree K				DSC based Enthalpy J/g	DSC based Entropy J/kg-K	Curie Temperature
Sample	e/a	x	A_s	A_f	M_s	M_f	Cooling	Cooling	T_C (K)
X5A	7.57	0.08	292	300	297	285	5.4	18.5	357
X5B	7.58	0.10	296	306	296	292	5.0	16.8	-
X5C	7.60	0.12	306	322	311	299	4.1	13.4	-
X2A	7.56	0.14	314	319	312	307	5.9	19.2	335
X2A SATC	7.56	0.14	314	321	312	308	4.9	15.8	-
X2B	7.59	0.16	336	343	334	326	9.1	27.6	340
X2B SATC	7.59	0.16	336	341	331	327	10.0	30.4	-
X5D	7.63	0.16	328	335	326	319	6.7	20.7	-
X2C	7.60	0.19	352	362	351	342	7.4	21.2	-
X2D	7.63	0.22	410	472	461	401	5.8	13.4	-
X2E	7.66	0.24	429	440	427	421	6.2	14.7	-

Graphical Abstract A-15-475-R2

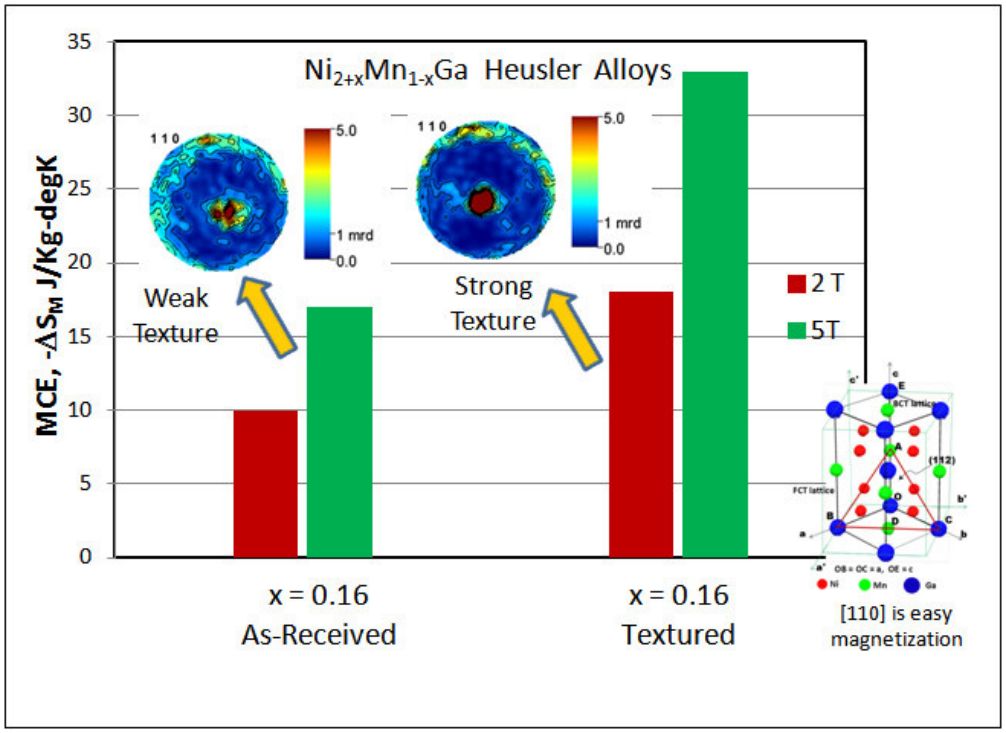

The picture portrays the influence of martensite texture on the magnetocaloric effect of alloy x = 0.16, which exhibited the best coincidence of structural and magnetic transformations.